available at www.sciencedirect.com

ScienceDirect

journal homepage: www.elsevier.com/locate/cherd

CFD simulation of particle deposition in a horizontal turbulent duct flow

Jinping Zhang [a,b,*], *Angui Li* [a]

[a] *School of Environmental and Municipal Engineering, Xi'an University of Architecture & Technology, Xi'an, Shanxi, China*
[b] *School of Environmental and Municipal Engineering, Lanzhou Jiaotong University, Lanzhou, Gansu, China*

ARTICLE INFO

Article history:
Received 21 March 2007
Accepted 5 October 2007

Keywords:
Turbulent duct flow
Computational fluid dynamics
Lagrangian eddy lifetime model
Dimensionless deposition velocities of particles
Reynolds-averaged Navier–Stokes equations
Dimensionless relaxing time

ABSTRACT

Deposition of particles in turbulent duct flows is crucial process in a number of industrial and environmental applications. Therefore, in this paper, particle deposition in a horizontal turbulent duct flow is simulated by CFD (computational fluid dynamics) modeling. Dimensionless deposition velocities of particles ranging from 10 to 200 μm are predicted by one-way coupling Lagrangian eddy lifetime model combined with a computation model of particle deposition in the turbulent duct flow with a fully developed velocity profiles based on RANS (Reynolds-averaged Navier–Stokes) equations at all three air speeds of 3.0, 5.0 and 7.0 m s^{-1}. It is shown that deposition rates (dimensionless deposition velocities) of particles to floors are higher than that to vertical wall and ceiling surfaces. Floor deposition rates increase with dimensionless relaxing time increasing, ceiling deposition rates decrease to zero with dimensionless relaxing time increasing, and wall deposition rates show the increase first and then a subtle decrease with dimensionless relaxing time increase at different air speeds. Wall and ceiling deposition rates increase with air speed increase at the same dimensionless relaxing time. Floor deposition rates decrease with air speed increase at the same dimensionless relaxing time. The simulation results are expected to be helpful for evaluating particle deposition rates in some environmental and industrial square ducts.

1. Introduction

Particle dispersion and deposition in turbulent bounded flows occur in numerous environmental and industrial applications. Contamination control, ventilation systems, gas cleaning, pneumatic transport, aerosol sampling, filtration and separation are but a few examples. The situation in some of these applications can be simplified as the deposition from a turbulent dispersed pipe flow, which can be regarded as a good beginning for studying this complex two-phase flow phenomenon. Straight horizontal square ducts may be components of these systems and they are common in ventilation systems. For flows of ducts in ventilation systems are usually turbulent, particles can deposit on ducts owing to interactions with this turbulence, by gravitational setting and other mechanisms. In fact, ducts in ventilation systems have been observed by Wallin (1994) and Liu et al. (2003) to accumulate particulate deposits on their interior surfaces. The size distributions of such deposited dust particles have not been investigated in detail, but the total mass of the deposits in all cited studies is likely to have been dominated by very large particles, debris and fibers. Thereby, particles ranging from 10 to 200 μm are first studied in this paper.

Deposition rates of particles from turbulent flows can be influenced by a variety of factors including particle size, degree of air turbulence, the roughness and orientation of the deposition surface. Investigations into deposition from turbulent flows in some literature have utilized three main methods: physical experiments, Eulerian modeling, and Lagrangian simulations. Most methods have been developed for deposition to smooth vertical surfaces from vertical flows with a fully developed turbulent flow profile. However, in

* *Corresponding author at*: School of Environmental and Municipal Engineering, Lanzhou Jiaotong University, Anning West Road 88#, Lanzhou, Gansu, China. Tel.: +86 931 4956848.
E-mail address: zhangjinping@mail.lzjtu.cn (J. Zhang).
0263-8762/$ – see front matter
doi:10.1016/j.cherd.2007.10.014

Nomenclature

a	cross-dimension of the duct, m
A	the cross-sectional area of the duct, m^2
C_{ave}	time-averaged airborne particle concentration in ducts, m^{-3}
C_c	slip correction factor
C_D	drag coefficient
C_1, C_2	empirical constants
d_p	particle diameter, m
D_h	the duct hydraulic diameter, m
f	the Fanning friction factor
F_x	additional force term, $m\,s^{-2}$
G_k	production term of k equation
J	time-averaged particle flux to the surface, $m^{-2}\,s^{-1}$
k	fluctuation kinetic energy, $kg\,m\,s^{-1}$
k'	the mean microscale roughness height of the rough wall, m
Kn	the Knudsen number
$N_{dep,c}$, $N_{dep,w}$	particle deposition numbers to ceiling and wall
$N_{dep,f}$	particle deposition numbers to floor
N_{in}	total particle numbers in the inlet in the duct
p_1	the perimeter of the duct normal to the flow direction, m
$\bar{p}$	mean pressure, Pa
Re	relative Reynolds number
R_{ij}	Reynolds stress tensor, Pa
S	mode of change rate tensor for average stress
S_φ	source term of the general equation
t	time, s
u	fluid phase velocity, $m\,s^{-1}$
u_i	instantaneous velocity, $m\,s^{-1}$
$\bar{u}_i$	mean velocity, $m\,s^{-1}$
u_i'	the ith fluctuation velocity component, $m\,s^{-1}$
u_p	particle velocity, $m\,s^{-1}$
u^*	friction velocity, $m\,s^{-1}$
U_{ave}	average air speed in the axial direction, $m\,s^{-1}$
V_d	deposition velocity, $m\,s^{-1}$
$V_{d,c}$, $V_{d,w}$	ceiling deposition velocity, wall deposition velocity, $m\,s^{-1}$
$V_{d,f}$	floor deposition velocity, $m\,s^{-1}$
V_d^+	dimensionless deposition velocity
x_i	position

Greek symbols

ε	turbulence dissipation rate
Γ_ϕ	effective exchange coefficient for the dependent variable φ
φ	each of the three velocity components u, v, w, and the kinetic energy of turbulence k, turbulence dissipation rate ε
λ	the mean free path of gas molecules, m
μ	molecular viscosity of the fluid (dynamic viscosity of air), Pa s
μ_t	the turbulent dynamics viscosity, Pa s
ν	kinematic viscosity of air, $m^2\,s^{-1}$
ν_t	turbulent viscosity, $m^2\,s^{-1}$
ρ	constant mass density (air density), $kg\,m^{-3}$
ρ_p	particle density, $kg\,m^{-3}$
σ^k	empirical constant
τ^+	dimensionless particle relaxation time
Ω_{ij}	tensor of average rotating rate with ω_k of angular velocity in a rotary reference coordinate system

some systems, both horizontal and vertical surfaces are normally present. For a horizontal square duct, it has three distinct internal surfaces: the floor, the wall and the ceiling. Deposition rates of particle to these surfaces are expected to differ owing to the influence of gravity and other deposition mechanisms. Some reviews of the work related to experimental and theoretical analyses of particle deposition in turbulent flows were presented by Wood (1981), and Papavergos and Hedley (1984). Some experimental data regarding particle deposition from turbulent flows have been collected using a range of techniques of varying quality by Sehmel (1973), Liu and Agarwal (1974), Shobokshy (1983) and Cheong (1997). The experimental data for particle deposition from turbulent flows in vertical tubes obtained by Liu and Agarwal (1974) have proven valuable for evaluating the predictive capabilities of theoretical models and the data would provide estimates for expected particle deposition rates to vertical surfaces in turbulent duct flows. Nevertheless, most of the data of acceptable quality collected from tubes or ducts with hydraulic diameters much smaller than 100 mm and nearly all investigations in horizontal flows have examined deposition only to the duct floor.

The theoretical approaches for prediction of particle deposition in turbulent flows are Eulerian model and Lagrangian simulations. According to literature of Ganic and Mastanaiah (1981), Lee and Wiesler (1987), and Yang and Lee (1991), in Eulerian model, particles are usually assumed to move toward the adjacent wall by turbulent diffusion and then reach the wall by a free fight mechanism. Lagrangian simulation of particle deposition in a turbulent flow involves two steps. First, the flow field is mathematically described, and second, particles are released into the simulated flow and trajectories are tracked based on the prescribed equations of particle motion. It is usually assumed that the presence of particles in the fluid does not affect the structure of the turbulent flow. This assumption is termed the one-way coupling assumption, referring to the fact that the fluid affects the particle momentum, but the particles do not influence the momentum of the fluid. The first Lagrangian simulation of particle deposition using a flow field generated by DNS (direct numerical simulation) was that of McLaughlin (1989) who studied the deposition of particles with values of dimensionless relaxation times τ^+ in the range 2–6 in a simulated vertical channel flow with Reynolds number $Re = 4000$. Brooke et al. (1992, 1994) conducted Lagrangian particle tracking in a DNS-generated vertical channel flow with particles in the diffusion-impaction regime considering only the drag force. Wang and Squires (1996a,b) demonstrated the feasibility of particle simulations in LES (large eddy simulation)-generated channel flows. Uijttewaal and Oliemans (1996) performed Lagrangian simulations of particles in the inertia-moderated regime in vertical cylindrical-tube flows generated by both DNS and LES. The investigation of Zhang and Ahmadi (2000) mainly focused on differences in deposition between upward vertical flow and downward vertical flow owing to changes in the lift force; however, the study is unique in that is the only DNS-Lagrangian simulation that includes deposition to

a floor. Results of particle deposition from these Lagrangian simulations generally agree with the trends and magnitudes observed in experiments and most simulating methods used by the literature are usually DNS-Lagrangian or LES-Lagrangian simulation. Lagrangian simulations have proven extremely useful for investigating the behavior of particles in turbulent airflows. However, scarcely any simulations have been performed for analyzing particle deposition to a ceiling, wall and floor in horizontal rectangle turbulent duct flows. Therefore, prediction of deposition to duct walls and ceilings by Lagrangian simulation is very necessary for achieving a more complete understanding of particle deposition in turbulent duct flows. Particle deposition data from this paper can provide a theoretical and practical guide to achieving quantitative evaluations of particle deposition in horizontal square turbulent duct or relevant flows.

Though DNS is a complete time-dependent solution of the exact Navier–Stokes equations for turbulent flows, DNS is not completely feasible for complex practical engineering problems. LES is a way solving only for the large eddies and modeling the smaller scales results in mesh resolution requirements. In practical terms, however, extremely fine meshes are still required in LES. It is only due to the explosive increases in computer hardware performance coupled with the availability of parallel processing that LES can be considered for engineering calculations. The Reynolds-averaged Navier–Stokes (RANS) equations represent transport equations for the mean flow quantities only, with all the scales of the turbulence being modeled. The approach of permitting a solution for the mean flow variables greatly reduces the computational effort. The Reynolds-averaged approach is generally adopted for practical engineering calculations.

Therefore, in this paper, dimensionless deposition velocities of particles ranging from 10 to 200 μm to various internal surfaces in smooth horizontal square turbulent duct flows with fully developed velocity profiles based on the RSM (Reynolds stress transport model) at all air speeds of 3.0, 5.0 and 7.0 m s^{-1} are predicted by RANS-Lagrangian simulation of CFD code. Drag, lift force, gravity, inertial force and turbulent diffusions are considered in this simulation. The influence of particle size, relaxation time, air speed and surface orientation on predicted deposition rates (dimensionless deposition velocities) of particles is discussed.In this simulation, Eddy lifetime model of Lagrangian stochastic models is used to track particles in the flows laden with particles. Given initial conditions of velocity and position, the motion of a single particle is calculated by treating it as a series of interactions with discrete eddies having a characteristic size, lifetime and velocity. Meanwhile, 40,000 particles are tracked and a one-way coupling between particles and flow field is considered, corresponding to a small loading fraction of the dispersed phase in turbulent duct flows, which does not alter significantly the dynamics of the airflow. Thereby, one-way coupling Lagrangian eddy lifetime model of tracking particles in the flows based on RANS expressions combined with a computation model of particle deposition are used to predict particle deposition rates to various different orientation internal faces in smooth horizontal square turbulent duct flows.

2. Numerical method

The Navier–Stokes and continuity equations are solved using the finite volume method on an given shaped flow domain with appropriate boundary conditions, and the calculation of particle trajectories by solving the equations of motion for a given particle is also allowed within the CFD code. One-way coupling Lagrangian eddy lifetime model combined with a computation model of particle deposition is used to simulate particle deposition in a smooth horizontal square fully developed turbulent duct flow.

3. Turbulent airflow model

For air turbulence in a square duct, the RANS equations can get closure by the turbulence model. Some turbulent airflow fields in rectangle or square ducts were generated by RSM (Reynolds stress transport model) (Demuren and Rodi, 1984; Bradshaw, 1987). Others airflow fields in rectangle or square ducts were generated by Realizable k–ε model by Luo et al. (2003), etc. To verify which turbulent model is better to simulate airflow fields in square ducts and more profitable for predict particle deposition in these ducts, contour of mean streamwise velocity generated by RSM is compared with that obtained from Realizable k–ε model of the CFD code FLUENT and particle deposition are evaluated, respectively. The flow near the wall is modeled using the standard wall function. Convergent residuals of velocity components are all lesser than 10^{-6} using the finite volume method (FVM) within CFD code.

The governing equations of Realizable k–ε Model for steady, isothermal and incompressible fluid can be written in the general format as follows:

$$\frac{\partial}{\partial x_i}(\rho u_i \varphi) = \frac{\partial}{\partial x_i}\left(\Gamma_\varphi \frac{\partial \varphi}{\partial x_i}\right) + S_\varphi \tag{1}$$

where, φ represents each of the three velocity components u, v, w, and the kinetic energy of turbulence k, and the turbulence dissipation rate, ε, Γ_φ is effective exchange coefficient for the dependent variable, φ, and S_φ is source term of the general equation. For specific meanings of all parameters, see Table 1.where,

$$G_k = \mu_t S^2 \tag{2}$$

G_k is production term of k equation, and S is mode of change rate tensor for average stress.

$$S \equiv \sqrt{2 S_{ij} S_{ij}} \tag{3}$$

$$S_{ij} = \frac{1}{2}\left(\frac{\partial u_i}{\partial x_j} + \frac{\partial u_j}{\partial x_i}\right) \tag{4}$$

$$G_k = \mu_t \left\{ \begin{array}{l} 2\left[\left(\frac{\partial u}{\partial x}\right)^2 + \left(\frac{\partial v}{\partial y}\right)^2 + \left(\frac{\partial w}{\partial z}\right)^2\right] \\ +\left(\frac{\partial u}{\partial y} + \frac{\partial v}{\partial x}\right)^2 + \left(\frac{\partial u}{\partial z} + \frac{\partial w}{\partial x}\right)^2 + \left(\frac{\partial w}{\partial y} + \frac{\partial v}{\partial z}\right)^2 \end{array} \right\} \tag{5}$$

$$\mu_t = \frac{C_\mu \rho k^2}{\varepsilon} \tag{6}$$

where, μ_t is the turbulent dynamics viscosity, and C_1 and C_μ are not constants in Realizable k–ε model equations and they are defined as:

$$C_\mu = \frac{1}{A_0 + A_s U^*(k/\varepsilon)}, \quad C_1 = \max\left[0.43 + \frac{\xi}{\xi + 5}\right] \tag{7}$$

Table 1 – Variables of the general differential equation for Realizable k–ε model

Equation	φ	Γ_φ	S_φ
Continuous equation	1	0	0
Momentum equation for x direction	u	$\mu_{eff} = \mu + \mu_t$	$-\frac{\partial p}{\partial x} + \frac{\partial}{\partial x}\left(\mu_{eff}\frac{\partial u}{\partial x}\right) + \frac{\partial}{\partial y}\left(\mu_{eff}\frac{\partial v}{\partial x}\right) + \frac{\partial}{\partial z}\left(\mu_{eff}\frac{\partial w}{\partial x}\right)$
Momentum equation for y direction	v	μ_{eff}	$-\frac{\partial p}{\partial y} + \frac{\partial}{\partial x}\left(\mu_{eff}\frac{\partial u}{\partial y}\right) + \frac{\partial}{\partial y}\left(\mu_{eff}\frac{\partial v}{\partial y}\right) + \frac{\partial}{\partial z}\left(\mu_{eff}\frac{\partial w}{\partial y}\right)$
Momentum equation for z direction	w	μ_{eff}	$-\frac{\partial p}{\partial z} + \frac{\partial}{\partial x}\left(\mu_{eff}\frac{\partial u}{\partial z}\right) + \frac{\partial}{\partial y}\left(\mu_{eff}\frac{\partial v}{\partial z}\right) + \frac{\partial}{\partial z}\left(\mu_{eff}\frac{\partial w}{\partial z}\right)$
Momentum equation for turbulent flows	k	$\mu + (\mu_t/\sigma_k)$	$G_k - \rho\varepsilon$
Equation of turbulent kinetic energy dissipation	ε	$\mu + (\mu_t/\sigma_\varepsilon)$	$\rho C_1 S\varepsilon - \rho C_2 \varepsilon^2/(k + \sqrt{\mu\varepsilon/\rho})$

Table 2 – Some constants in Realizable k–ε model

A_0	C_2	σ_k	σ_ε
4.04	1.9	1.0	1.2

$$\xi = \frac{Sk}{\varepsilon}, \quad U^* \equiv \sqrt{S_{ij}S_{ij} + \tilde{\Omega}_{ij}\tilde{\Omega}_{ij}} \tag{8}$$

$$\tilde{\Omega}_{ij} = \Omega_{ij} - 2\varepsilon_{ij}\omega_k, \quad \Omega_{ij} = \overline{\Omega_{ij}} - \varepsilon_{ijk}\omega_k \tag{9}$$

where, Ω_{ij} is tensor of average rotating rate with ω_k of angular velocity in a rotary reference coordinate system.

$$A_s = \sqrt{6}\cos\phi, \quad \phi = \frac{1}{3}\arccos(\sqrt{6}W), \quad W = \frac{S_{ij}S_{jk}S_{ki}}{\tilde{S}}, \quad \tilde{S} = \sqrt{S_{ij}S_{ij}} \tag{10}$$

For other constants in Realizable k–ε model equations, see Table 2.

The equations are discretized into algebraic equations by the finite volume method (FVM). The discretization method is a Quick scheme and SIMPLE algorithm is adopted.

For an incompressible fluid, the equations of continuity and balance of momentum for the mean motion are given as

$$\frac{\partial \bar{u}_i}{\partial x_i} = 0 \tag{11}$$

$$\frac{\partial \bar{u}_i}{\partial t} + \bar{u}_j\frac{\partial \bar{u}_i}{\partial x_j} = -\frac{1}{\rho}\frac{\partial \bar{p}}{\partial x_i} + \nu\frac{\partial^2 \bar{u}_i}{\partial x_j \partial x_j} - \frac{\partial}{\partial x_j}R_{ij} \tag{12}$$

where $\bar{u}_i$ is the mean velocity, x_i is the position, t is the time, $\bar{p}$ is the mean pressure, ρ is the constant mass density, ν is the kinematic viscosity, and $R_{ij} = \overline{u_i' u_j'}$ is the Reynolds stress tensor. Here, $u_i' = u_i - \bar{u}_i$ is the ith fluctuation velocity component, and u_i is the instantaneous velocity.

The Reynolds stress model (RSM) involves calculation of the individual turbulence stresses via a differential transport equation given as

$$\underbrace{\frac{\partial}{\partial t}R_{ij} + \bar{u}_k\frac{\partial}{\partial x_k}R_{ij}}_{\text{convective transport}} = \underbrace{+\frac{\partial}{\partial x_k}\left(\frac{\nu_t}{\sigma^k}\frac{\partial}{\partial x_k}R_{ij}\right)}_{\text{diffusive transport}} \underbrace{-\left[\overline{u_i'u_k'}\frac{\partial \bar{u}_j}{\partial x_k} + \overline{u_j'u_k'}\frac{\partial \bar{u}_i}{\partial x_k}\right]}_{P_{ij}=\text{production}}$$
$$\underbrace{-C_1\frac{\varepsilon}{\kappa}\left[R_{ij} - \frac{2}{3}\delta_{ij}\kappa\right] - C_2\left[P_{ij} - \frac{2}{3}\delta_{ij}P\right]}_{\phi_{ij}=\text{pressure strain}} \underbrace{-\frac{2}{3}\delta_{ij}\varepsilon}_{\varepsilon_{ij}=\text{dissipation}} \tag{13}$$

where the production is given as

$$P_{ij} = -\overline{u_i'u_k'}\frac{\partial \bar{u}_j}{\partial x_k} - \overline{u_j'u_k'}\frac{\partial \bar{u}_i}{\partial x_k}, \quad P = \frac{1}{2}P_{ii} \tag{14}$$

where, ν_t is turbulent viscosity, $\sigma^k = 1.0$, $C_1 = 1.8$ and $C_2 = 0.6$ are empirical constants.

$k = (1/2)\overline{u_i'u_j'}$, is the fluctuation kinetic energy by Launder et al. (1975), and ε is the turbulence dissipation rate.

The turbulence dissipation rate ε, is computed by the governing equation:

$$\frac{\partial \varepsilon}{\partial t} + \bar{u}_j\frac{\partial \varepsilon}{\partial x_j} = \frac{\partial}{\partial x_j}\left[\left(\nu + \frac{\nu_t}{\sigma^\varepsilon}\right)\frac{\partial \varepsilon}{\partial x_j}\right] - C^{\varepsilon 1}\frac{\varepsilon}{\kappa}R_{ij}\frac{\partial \bar{u}_i}{\partial x_j} - C^{\varepsilon 2}\frac{\varepsilon^2}{\kappa} \tag{15}$$

The values of constants are given by Rodi (1984) as follows:

$$\sigma^\varepsilon = 1.3, \quad C^{\varepsilon 1} = 1.44, \quad C^{\varepsilon 2} = 1.92 \tag{16}$$

Here, $\nu_t = \mu_t/\rho$, expression of μ_t can be seen from Eq. (6), and $C_\mu = 0.09$.

More details and the turbulence parameters for the Reynolds stress model can be found from Launder et al. (1975) and Fluent (2002).

The RSM from the CFD code uses the standard wall function for calculating the mean velocity field and the components in turbulent flows. Convergent residuals of velocity components and Reynolds stress components are lesser than 10^{-6} using the finite volume method (FVM) within CFD code. The discretization method is a second-order upwind scheme and SIMPLE algorithm is adopted.

4. Boundary conditions of air phase

Since turbulent airflow considered in the simulation is a fully developed flow, periodic boundary conditions (specified mass flow rate and pressure drop) at the inlet are imposed in the original flow field computation. When the discrete phase model is used, as used by Pushkar and Michael (1998) and Qian and Goodarz (1997), velocity-inlet boundary conditions and outflow boundary conditions are imposed at the same duct, i.e., the airflow velocity profiles at the duct flow are described according to the results of periodic boundary conditions. No-slip boundary conditions are assumed at the walls.

5. Particle trajectory model

A Lagrangian stochastic model, i.e., Lagrangian eddy lifetime model is employed in the particle trajectory calculation. The deposition rates of particles of various diameters (10, 15, 20, 30, 50, 70, 80, 100, 120, 150, 180 and 200 μm) at all three air speeds of 3.0, 5.0 and 7.0 m s^{-1} are predicted in smooth horizontal square fully developed turbulent duct flows. The Lagrangian approach splits the particle phase into a representative set of individual particles and tracks these particles separately through the flow domain by solving the equations of particle movement.

The following assumptions are used: (a) no particle rebounds on solid surfaces; (b) particle concentrations are assumed be low enough to ignore particle–particle interactions; (c) all particles are in spherical solid shape.

6. Motion equations of particle

The trajectory of a discrete phase particle is tracked by integrating the force balance on the particle, which is written in a Lagrangian reference frame. Drag, gravitational setting, Saffman lift force and turbulent diffusions are considered in the process of computation. It can be written (for the x direction in Cartesian coordinates) as

$$\frac{du_p}{dt} = F_D(u - u_p) + \frac{g_x(\rho_p - \rho)}{\rho_p} + F_x \quad (17)$$

where $F_D(u - u_p)$ is the drag force per unit particle mass and

$$F_D = \frac{18\mu}{\rho_p d_p^2}\frac{C_D Re}{24} \quad (18)$$

where, u is the fluid phase velocity, u_p is the particle velocity, ρ is the air density, ρ_p is the density of the particle, and d_p is the particle diameter. Re is the relative Reynolds number and C_D is the drag coefficient. Re and C_D are defined as expressions of Morsi and Alexander (1972).

The $g_x(\rho_p - \rho)/\rho_p$ term, in Eq. (17) represents gravity term and F_x is the additional force term. Because the gravity force is included in this simulation, the magnitude and direction of the gravity vector need to be defined. Forces acting on the particle, i.e., deposition mechanisms of particle in a turbulent flow duct usually include gravity, inertial force and drag force. In addition, Brown force, turbulent diffusion, Saffman force, thermophoresis force and electrostatic drift can be also included in the turbulent flow duct. Due to the particles investigated in this paper are larger than 5 μm, Brown force, thermophoresis force and electrostatic drift may be omitted. The CFD code predicts the turbulent dispersion of particles by integrating the trajectory equations for individual particles, using the instantaneous fluid velocity along the particle path during the integration. By computing the trajectory in this manner for a sufficient number of representative particles, the trajectories computed will include a statistical representation of the spread of the particle stream due to turbulence. Therefore, the random effects of turbulence on the particle dispersion may be accounted for. In the simulation, the Eddy lifetime model (one-way coupling eddy–particle interaction model) from FLUENT is used. The fluctuating velocity components are discrete piecewise constant functions of time. Their random value is kept constant over an interval of time given by the characteristic lifetime of eddy.

Thereby, the additional force term, F_x, in Eq. (17) include only a Saffman's lift force. The lift force is calculated according to the expressions of FLUENT code provided by Saffman (1965).

7. Boundary and initial conditions of particle phase

A particle will be trapped if it contacts a duct wall and the particle will escape if it reaches an inlet or outlet boundary.

The initial conditions of a particle include position of the particle, velocities of the particle and diameter of the particle, etc.

A sample of 40,000 particles with diameter of 10–200 μm is considered in this simulation. The particles distributed with equal space for each diameter are injected from a plane in the inlet of the duct. The velocities of the particles are assumed be the same as the fluid velocity. The particle density is 1500 kg m^{-3}.

8. Computation of particle deposition rates

Particle deposition rates predicted by models are most commonly expressed in terms of the dimensionless deposition velocity, V_d^+. The deposition velocity, V_d of a particle to a duct surface is defined as

$$V_d = \frac{J}{C_{ave}} \quad (19)$$

where J is the time-averaged particle flux to the surface and C_{ave} is the time-averaged airborne particle concentration in a turbulent duct flow.

The dimensionless particle deposition velocity V_d^+ defined by normalizing the deposition velocity with the friction velocity, u^*.

$$V_d^+ = \frac{V_d}{u^*} \quad (20)$$

The friction velocity of a turbulent duct flow, u^*, can be calculated according to the formulas from Anand et al. (1993).

$$u^* = U_{ave}\sqrt{\frac{f}{2}} \quad (21)$$

where, U_{ave} is the average air speed in the axial direction, A is the cross-sectional area of the duct, f is the Fanning friction factor. For fully developed turbulent flow in a smooth- or rough-walled duct, f can be calculated using the following equation from White (1986):

$$\frac{1}{\sqrt{f}} = -3.6\log\left[\frac{6.9}{Re} + \left(\frac{k'}{3.7D_h}\right)^{1.11}\right] \quad (22)$$

where, k' is the mean microscale roughness height of the rough wall and Re is the Reynolds number of the duct flow calculated by

$$Re = \frac{D_h U_{ave}}{\nu} \quad (23)$$

where, ν is the kinematic viscosity of air. The duct hydraulic diameter, D_h, is defined by this expression:

$$D_h = \frac{4A}{p_1} \quad (24)$$

where, A is the cross-sectional area of the duct, and p_1 is the perimeter of the duct normal to the flow direction.In a horizontal square duct, it has three distinct internal surfaces: the floor, the wall and the ceiling. Deposition velocities of particle to these surfaces are expected to differ owing to the influence

of gravity. Models for predicting particle loss through a series of straight tubes have been proposed by Brockman (2001) and Anand et al. (1993). Author in this paper deduces the expressions of particle deposition velocities to the ceiling, vertical wall and floor in a horizontal rectangle duct according to the reference of Brockman (2001) and Anand et al. (1993).

According to the number of particles injected in the inlet plane and the number of particles deposited to the floor, the wall and the ceiling, particle deposition velocities to the floor, the wall and the ceiling may be, respectively, calculated in a horizontal square straight duct.

$$V_{d,c} = -\frac{aU_{ave}\ln(1 - N_{dep,c}/N_{in})}{L} \quad (25)$$

$$V_{d,w} = -\frac{aU_{ave}\ln(1 - N_{dep,w}/N_{in})}{2L} \quad (26)$$

$$V_{d,f} = -\frac{aU_{ave}\ln(1 - N_{dep,f}/N_{in})}{L} \quad (27)$$

where, U_{ave} is the average air speed in the axial direction, a is the cross-dimension of the duct and L is the duct section length. $V_{d,c}$, $V_{d,w}$ and $V_{d,f}$ are separately ceiling deposition velocity, wall deposition velocity and floor deposition velocity. $N_{dep,c}$, $N_{dep,w}$ and $N_{dep,f}$ are separately particle deposition numbers to ceiling, wall and floor. N_{in} is total particle numbers in the inlet in the duct.

In studies of particle deposition from turbulent flows, it is common to investigate the relationship between the dimensionless particle deposition velocity and the dimensionless particle relaxation time. The relaxation time of a particle, τ_p, is the characteristic time for a particle velocity to respond to a change in air velocity. It may be calculated for spherical particles in the Stokes flow regime as follows:

$$\tau_p = \frac{C_c\rho_p d_p^2}{18\mu} \quad (28)$$

where C_c is the Cunningham slip correction factor and μ is the dynamic viscosity of air. The slip correction factor can be estimated by the expression

$$C_c = 1 + Kn\left[1.257 + 0.4\exp\left(-\frac{1.1}{Kn}\right)\right] \quad (29)$$

where the Knudsen number, Kn, is

$$Kn = \frac{2\lambda}{d_p} \quad (30)$$

and λ is the mean free path of gas molecules, equal to 0.065 μm at a temperature of 25 °C and atmospheric pressure.

Turbulent eddies in duct flows display a wide range of length scales, with the largest eddies limited by the duct dimensions and the smallest limited by the dissipative action of molecular viscosity. Smaller eddies tend to be shorter lived while larger eddies persist or a longer time before disappearing. The smallest eddies in a flow are those near the walls and their average lifetime may be estimated by

$$\tau_e = \frac{\nu}{u^{*2}} \quad (31)$$

Because deposition happens at walls, particle interactions with near-wall eddies are potentially important in determining deposition rates. A dimensionless particle relaxation time, τ^+, can be defined by comparing the particle relaxation time to the timescale associated with the near-wall turbulent eddies. A dimensionless particle relaxation time, τ^+, may be calculated for spherical particles in the Stokes flow regime as follows:

$$\tau^+ = \frac{\tau_p}{\tau_e} = \frac{C_c\rho_p d_p^2 u^{*2}}{18\mu\nu} \quad (32)$$

9. Particle deposition mechanism

Particles can reach a duct wall surface in two ways: direct inertial impact and boundary layer diffusion. Direct inertial impact occurs when a particle may not follow the flow and deviates significantly from the curved flow streamlines to collide on the surface. For a given flow, inertial effects increase with increasing particle size. Particle deposition by turbulent diffusion and inertial impaction has been studied theoretically by Fackrell et al. (1994). They found that when the particles do not undergo significant direct impact, inertial effects still influence their diffusive deposition. This means that the two type of particle transporting mechanisms inertial and turbulent diffusion have to be studied together. One of the models that simulate the effect of the turbulence on the particle trajectories is the eddy lifetime. This model had been used successfully in pervious work of Greenfield and Quarini (1997). They modeled the turbulence as a series of random eddies that have a lifetime and associated random fluctuating velocities. In this paper, the same eddy lifetime model is used. By computing the trajectory for a sufficient number of representative particles, the random effects of turbulence on the particle dispersion may be taken into account.

10. Study of a turbulent duct flow case

To simulate particle deposition in a square turbulent duct flow, a smooth straight horizontal square duct with a fully developed turbulent flow profile is investigated in detail. The primary flow considered in a vertical duct with a square cross-section of 10 cm × 10 cm and a length of 2 m is a fully developed turbulent flow.

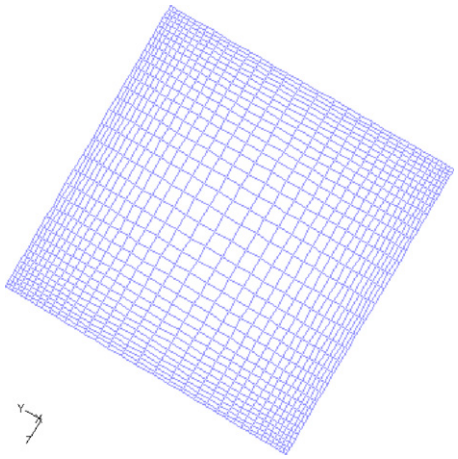

Fig. 1 – A cross-section grid of a horizontal square duct flow.

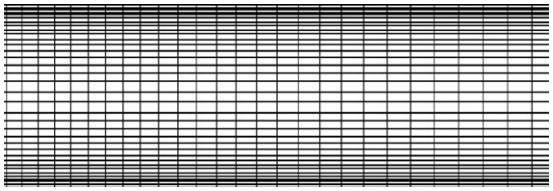

Fig. 2 – Streamwise grid of a horizontal square turbulent duct flow.

Figs. 1 and 2 show schematics of the computational grid of the duct geometry. The grid is non-uniform and is denser near the wall where the velocity gradients were expected to be the highest.

11. Results and analyses

11.1. *Airflow field*

Figs. 3 and 4 show the streamwise velocity contours generated by Realizable k–ε model at air speeds of 5.0 and 7.0 m s^{-1}. Figs. 5–7 display the streamwise velocity contours generated by RSM at air speeds of 3.0, 5.0 and 7.0 m s^{-1}. From Figs. 3 and 4, it is observed that mean streamwise contours don't bulge towards the corners and are similar to streamwise contours generated in round pipes. It is noticed that the velocity near the duct center is highest. It is also seen that mean streamwise contours bulge towards the corners from Figs. 5–7. This phenomena illustrates mean secondary flows may be produced in the square duct. The reason of secondary flows generation is possibly velocity fluctuations tangential to streamwise velocity contours in regions of contour curvature cause a transverse mean flow that is directed towards the corners or secondary flows are caused by the gradients in the Reynolds stresses. It is agreement with the previous LES results of study on secondary flows in a square duct that were performed by Madabhushi and Vanka (1991) and Chad (2002). At the same air speed, the difference of velocity magnitude predicted by two models is not too obvious.

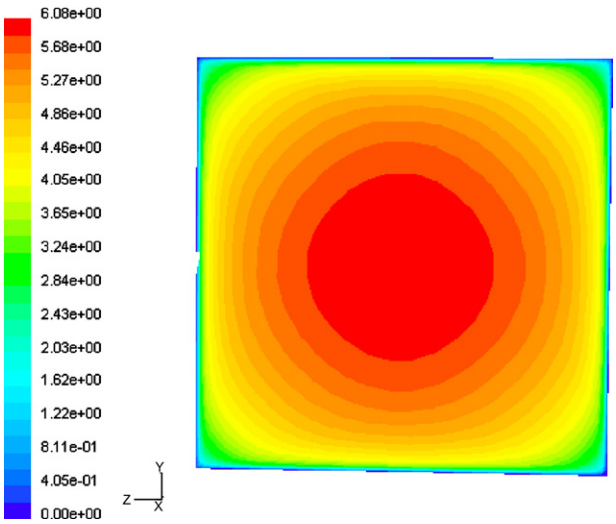

Fig. 3 – Contours of streamwise velocity generated by Realizable k–ε model of a horizontal square duct at 5 m s^{-1}.

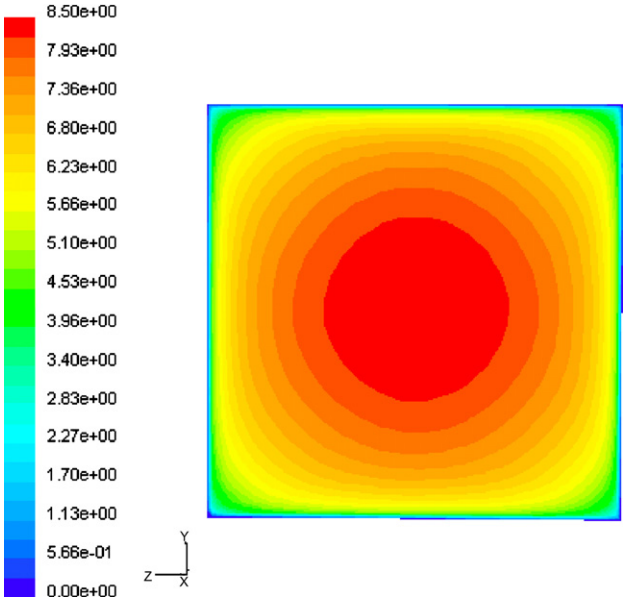

Fig. 4 – Contours of streamwise velocity generated by Realizable k–ε model of a horizontal square duct at 7 m s^{-1}.

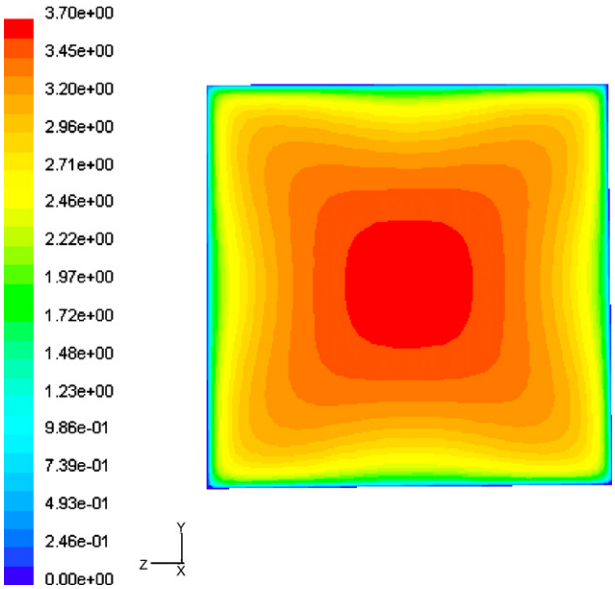

Fig. 5 – Contours of streamwise velocity generated by RSM of a horizontal square duct at 3 m s^{-1}.

12. Particle deposition rates

Figs. 8–10 display predicted dimensionless ceiling, wall and floor deposition velocities from fully developed turbulent flow in a smooth horizontal square duct by the Realizable k–ε model at air speed of 5 m s^{-1}. In Figs. 8–10, it is recognized that ceiling, wall and floor deposition rates of particles in a smooth horizontal square duct flow generated by a Realizable k–ε turbulence model are all slightly greater than that by RSM.

In fact, it is very difficult to decide which turbulent airflow model is more reasonable for predicting deposition rates of particles, whereas from velocity contours of flow field, RSM is more suitable as the model of calculating flow field. In Figs. 11–16, predicted dimensionless deposition velocities to the duct floor, sidewall and ceiling of a smooth horizontal square duct

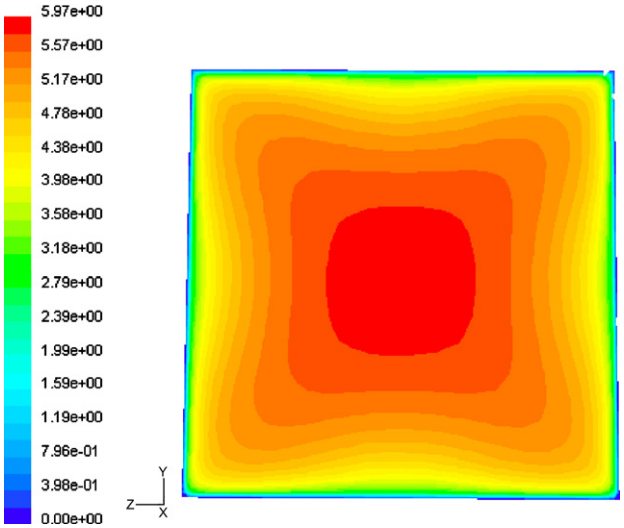

Fig. 6 – Contours of streamwise velocity generated by RSM of a horizontal square duct at 5 m s^{-1}.

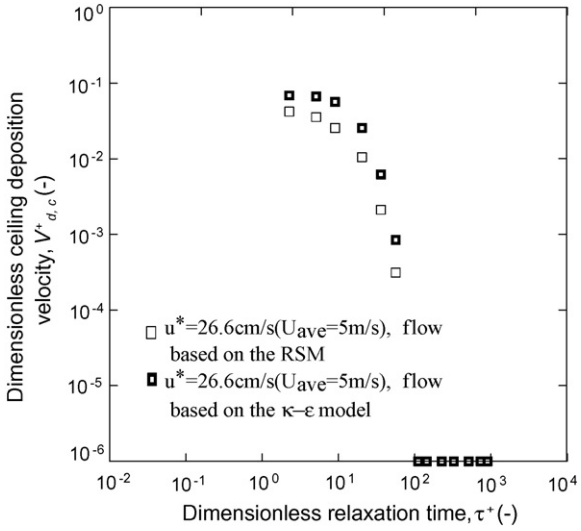

Fig. 8 – Comparison of dimensionless ceiling deposition velocities predicted from a horizontal flow based on the RSM and the Realizable k–ε model at 5 m s^{-1}.

flow by the RSM are presented graphically. Figs. 11–13, respectively, show predicted dimensionless ceiling, wall and floor deposition velocities versus dimensionless relaxing time at all air speeds of 3.0, 5.0 and 7.0 m s^{-1}.

Fig. 14 shows predicted dimensionless ceiling deposition velocities at all air speeds. Due to no relevant deposition data are reported, no available data from the literature are compared with them. Predicted dimensionless sidewall deposition velocities at all air speeds are compared with the vertical-wall deposition experimental data collected by Liu and Agarwal (1974) and simulated by Uijttewaal and Oliemans (1996) in a vertical channel in Fig. 15. Fig. 16 compares predicted dimensionless floor deposition velocities at three air speeds with floor deposition data from Sehmel (1973) and Zhang and Ahmadi (2000) in a horizontal channel.

From Figs. 11–13, for a dimensionless relaxing time at given air speed, the dimensionless deposition velocity to the duct floor is greater than the deposition rate to the duct wall, which,

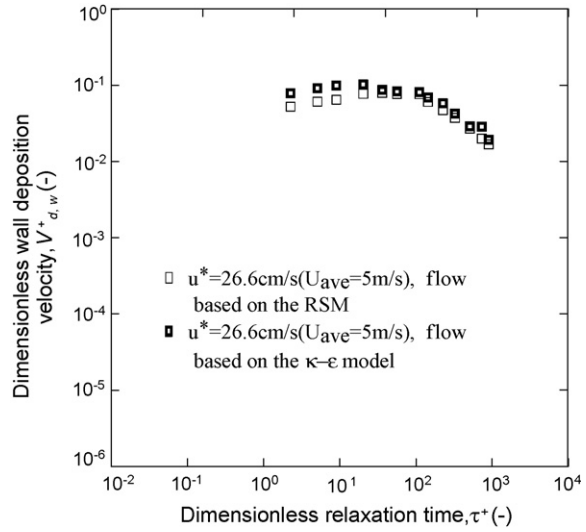

Fig. 9 – Comparison of dimensionless wall deposition velocities predicted from a horizontal flow based on the RSM and the Realizable k–ε model at 5 m s^{-1}.

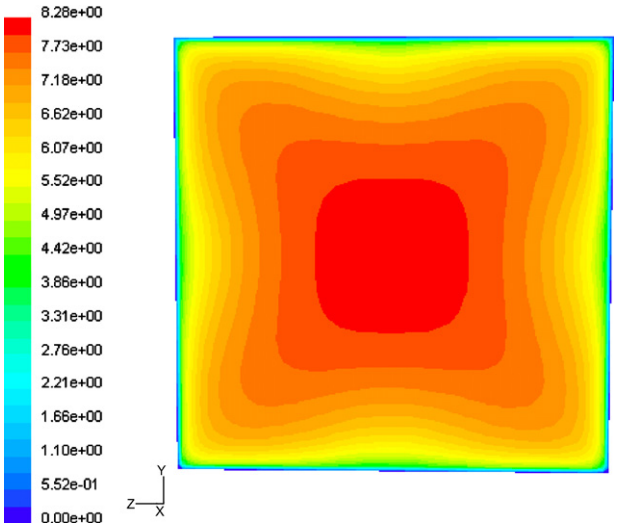

Fig. 7 – Contours of streamwise velocity generated by RSM of a horizontal square duct at 7 m s^{-1}.

in turn, is greater than the deposition rate to the duct ceiling. Data at the lowest air speed of 3 m s^{-1} show dimensionless deposition velocities to the duct floor are greater than deposition rates to the ceiling by factors in the ranges 1.8–312, and greater than deposition rates to the wall by factors in the ranges 1.4–4.1 for $0.9 < \tau^+ < 8.3$. Deposition rates to the duct floor are 1–3 orders of magnitude greater than deposition rates to the wall for $8.3 < \tau^+ < 369$, whereas deposition rates to the ceiling quickly decrease to zero as τ^+ is equal to 45.2. The differences in deposition rates to the duct floor, wall and ceiling decrease with increasing air speed, as can be seen by the grouping of the data for the different surfaces in Figs. 12 and 13 as compared to Fig. 11.

The current simulation results of wall deposition are both in the diffusion-impaction regime and the inertia-moderated regime, whereas mainly are in inertia-moderated regime according to the literature from Papavergos and Hedley (1984).

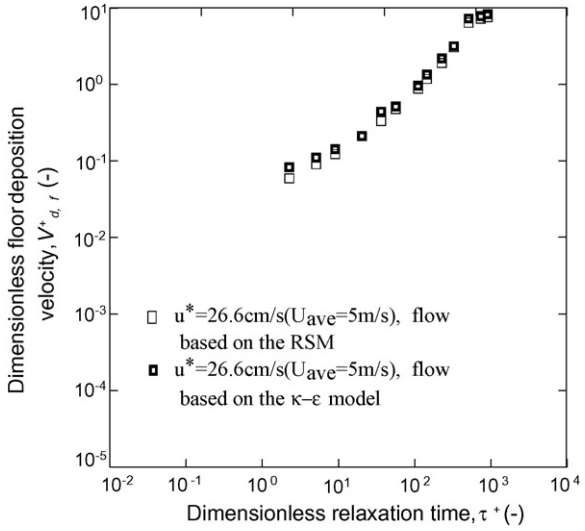

Fig. 10 – Comparison of dimensionless floor deposition velocities predicted from a horizontal flow based on the RSM and the Realizable k–ε model at 5 m s^{-1}.

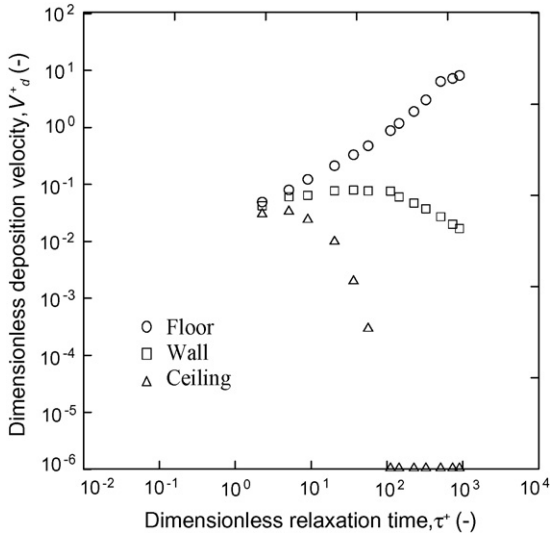

Fig. 12 – Predicted dimensionless deposition velocities for particles depositing to the floor, wall and ceiling in a smooth horizontal square duct flow at 5 m s^{-1}.

Floor deposition rates increase with dimensionless relaxing time τ^+ increase, whereas ceiling deposition rates first gradually decrease and then rapidly decrease to zero with τ^+ increase at three different air speeds. Wall deposition rates increase first with dimensionless relaxing time τ^+ increase and then slightly decrease with τ^+. The data display the trend of decreasing wall deposition rates with increasing particle dimensionless relaxing time in the certain range of inertia-moderated regime at three different air speeds. Because these particles are very large, their motion is not significantly influenced by flows in the near-wall region. Instead it is dominated by larger eddies in the turbulent core. Very large particles may lead to wall deposition rates decrease in the inertia-moderated regime as the decreased response to turbulent velocity fluctuations of large particles.

In Fig. 14, comparing predicted dimensionless ceiling deposition rates at three different air speeds, for similar values of dimensionless relaxing time, τ^+, dimensionless

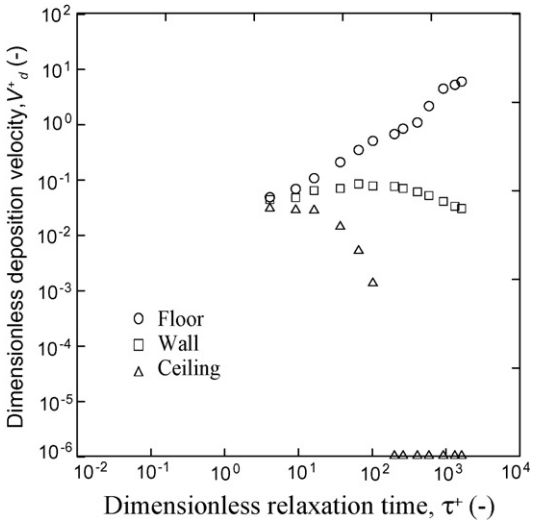

Fig. 13 – Predicted dimensionless deposition velocities for particles depositing to the floor, wall and ceiling in a smooth horizontal square duct flow at 7 m s^{-1}.

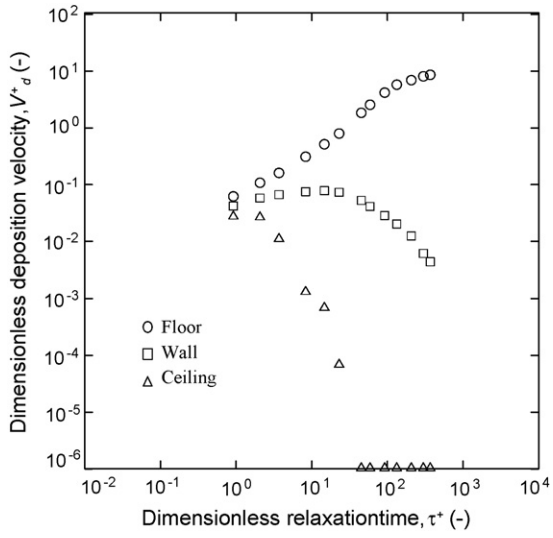

Fig. 11 – Predicted dimensionless deposition velocities for particles depositing to the floor, wall and ceiling in a smooth horizontal square duct flow at 3 m s^{-1}.

ceiling deposition velocities are greatest at the largest air speed of 7 m s^{-1}. This may be due to increased air speeds result in increasing of turbulent intensity. Ceiling deposition rates all have a rapidly decreased tendency with τ^+ increasing at three different air speeds. For the phenomena, it can be explained by the writers from this paper. For smaller particles, the turbulent diffusion, Brown diffusion and other mechanisms may be the dominant mechanisms for particle deposition to the duct ceiling. The gravitational sedimentation effect becomes more important as particle size increases to very large. In general, for particles greater than 5 μm, the gravitational sedimentation is the dominant mechanism for particle deposition in a horizontal duct. The turbulent diffusion and Brown diffusion have unimportant effect on deposition of larger particles. Due to probability of collision of larger particles to the ceiling become smaller, particles mainly deposit to the floor and scarcely deposit to the ceiling. Hence,

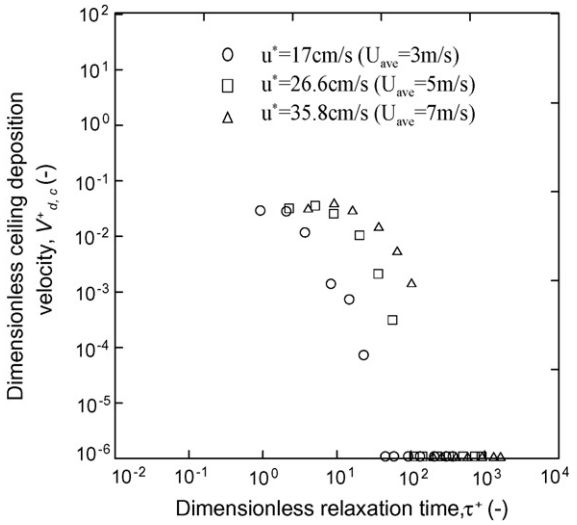

Fig. 14 – Comparison of dimensionless ceiling deposition velocities predicted at three air speeds in a smooth horizontal square duct flow.

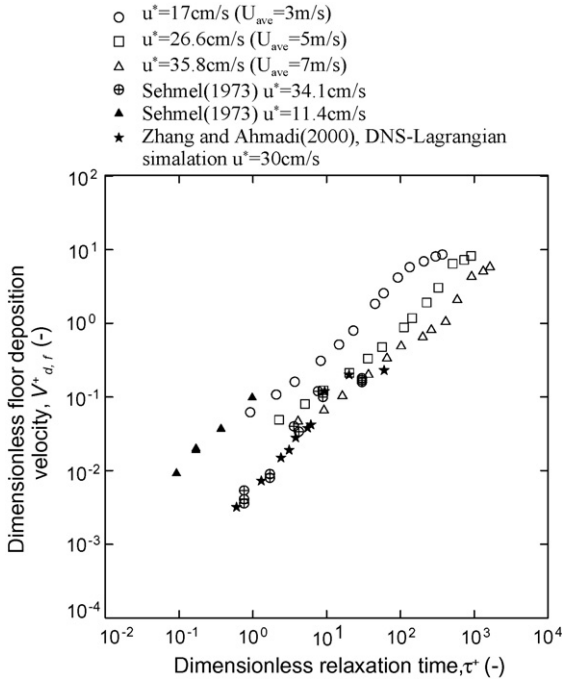

Fig. 16 – Comparison of dimensionless floor deposition velocities predicted at three air speeds in a smooth horizontal square duct flow with the data of Sehmel (1973) and Zhang and Ahmadi (2000).

that deposition rates of particles for 10–200 μm to the ceiling decrease with dimensionless relaxation time increasing is reasonable. Ceiling deposition rates rapidly decrease to zero with particle diameter increasing to very large. At three air speeds of 3.0, 5.0 and 7.0 m s^{-1}, dimensionless relaxation time, respectively, is 45.2, 111 and 200 corresponding to 0.0 values of dimensionless ceiling deposition velocities.

The data of dimensionless wall deposition velocity, $V^{+}_{d,w}$, versus dimensionless relaxing time, τ^{+}, at three different air speeds is presented graphically in Fig. 15. In the figure, predicted wall deposition rates are compared with the data of Liu and Agarwal (1974) and Uijttewaal and Oliemans (1996) with $Re = 5300$. The data of Liu and Agarwal (1974) were collected at a friction velocity of about 74 cm s^{-1}. Reasonable agreement at three friction velocities is observed in the diffusion-compaction regime and the inertial-moderated region. The simulated data are slightly larger than wall

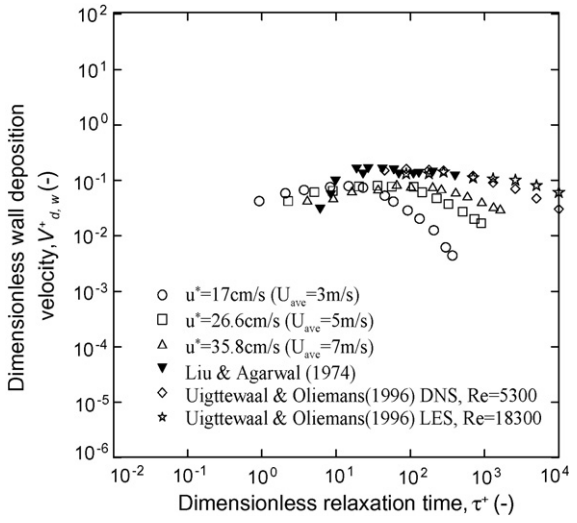

Fig. 15 – Comparison of dimensionless wall deposition velocities predicted at three air speeds in a smooth horizontal square duct flow with the data of Liu and Agarwal (1974) and Uijttewaal and Oliemans (1996).

deposition rates from the literature. The reason is that wall deposition rates of vertical ducts are greater than that in horizontal ducts at the same parameters. The data from Liu and Agarwal (1974) and from Uijttewaal and Oliemans (1996) are obtained in vertical ducts. Wall deposition rates increase with friction velocity, u^{*}, increase for the same τ^{+}. This indicates dimensionless wall deposition velocities rely on the magnitude of the friction velocity. The effect is may caused by deposition of large particles to the wall that is dominated by inertia effect. Inertia of large particles is enhanced with increasing air speeds. In Fig. 16, comparing predicted dimensionless floor deposition velocities with other floor deposition data from the literature, good agreement among the data is observed for common friction velocities. Data obtained at the lowest air speed of 3 m s^{-1} with a nominal friction velocity of 0.170 m s^{-1} comparison with data collected by Sehmel (1973) at a friction velocity of 0.114 m s^{-1} exhibit a similar slope. Data obtained at the highest air speed of 7 m s^{-1} with a nominal friction velocity of 0.358 m s^{-1} also display a similar slope comparing with the data from Sehmel (1973) at a friction velocity of 0.341 m s^{-1} and the data from Lagrangian simulation based on the DNS in Zhang and Ahmadi (2000). Fig. 16 shows that dimensionless floor deposition velocities are larger at lesser air speed of 3 m s^{-1}, and particles deposit to the floor in a nearly uniform manner at three different air speeds. Dimensionless floor deposition velocity in the horizontal duct increases with dimensionless relaxing time increasing. However, as particle diameter increase to very large, the floor deposition velocity increase very slowly and approach leveling. This is due to gravitational setting dominates deposition of particles to the floor and gradually absolutely dominates floor deposition of particles. It is observed from Fig. 16, dimensionless floor deposition velocities decrease with friction velocity, u^{*}, increase at the same τ^{+}.

13. Discussion and conclusions

Though it is difficult to decide which airflow model is more reasonable for predicting deposition rates of particles to the ceiling, wall and floor from fully developed turbulent flows in smooth square horizontal ducts, however, from velocity contours of flow field, RSM seem to be more suitable as the model of airflow field. The predicted results are expected to be helpful for evaluating particle deposition rates in some environmental and industrial square ducts. Based on the presented results, the following conclusions may be drawn for particles ranging from 10 to 200 μm:

- The simulation results are agreeable with the available experimental data and the numerical results from the literature for fully developed turbulent flows.
- In smooth horizontal square turbulent duct flows, dimensionless deposition velocities (deposition rates) of particles to the floor are higher than to the wall or the ceiling at different air speeds. The differences in deposition rates to the floor, wall and ceiling decrease with increasing air speed.
- Floor deposition rates increase with dimensionless relaxing time increasing, whereas ceiling deposition rates decrease to zero with dimensionless relaxing time increasing at different air speeds.
- Wall deposition rates show the increase with dimensionless relaxing time or particle size in the range of diffusion-compaction regime and a subtle decrease with dimensionless relaxing time or particle size increase in the range of inertia-moderated regime at different air speeds. Wall and ceiling deposition rates increase with friction velocity increase at the same dimensionless relaxing time.
- Floor deposition rates decrease with friction velocity increase in friction velocity at the same dimensionless relaxing time. Floor deposition rates increase with dimensionless relaxation time increasing.
- Deposition rates to the floor, wall and ceiling are mainly dependent on the magnitude of the friction velocity and particle diameter, and are relevant to many factors.
- It is the first to simulate particle deposition rates adequately to the ceiling, wall and floor and compare the magnitude of deposition rates to various faces using the Lagrangian eddy lifetime model based on flows by RANS expressions.

For a more complete understanding of particle deposition in turbulent duct flows, more simulations and experiments are still needed in various square and rectangle ducts.

Acknowledgement

The authors would like to acknowledge financial support from The National Nature Science Foundation of China (No. 50478046).

REFERENCES

Anand, N.K., McFarland, A.R., Wong, F.S. and Kocmoud. C.J., 1993, Deposition: software to calculate particle penetration through aerosol transport systems (NUREG/GR-0006, Nuclear Regulatory Commission, Washington, DC).

Brooke, J.W., Kontomaris, K., Hanratty, T.J. and McLaughlin, J.B., 1992, Turbulent deposition and trapping of aerosols at a wall, Phys Fluids A, 4: 825–834.

Brooke, J.W., Hanratty, T.J. and McLaughlin, J.B., 1994, Free flight mixing and deposition of aerosols, Phys Fluids A, 6: 3404–3415.

Brockman, J.E. 2001, Sampling and transport of aerosols, In P. A. Baron & K. Willeke (Eds.), Aerosol Measurement: Principles, Techniques and Applications (2nd ed., pp. 259–276). New York: John Wiley.

Bradshaw, P. 1987, Turbulent secondary flows, Fluid Mech, 19: 53–74.

Cheong, K.W. 1997, Deposition of aerosol particles in ductwork, Appl Energy, 57: 253–261.

Chad, M.W., 2002, Large eddy simulations of particle dispersion and deposition in a turbulent square duct flow, Ph.D. Dissertation (Mechanical Engineering, University of Illinois, Urbana-Champaign).

Demuren, A.O. and Rodi, W., 1984, Calculation of turbulent-driven secondary motion in non-circular ducts, J Fluid Mech, 140: 189–222.

Fackrell, J.E., Tabberer, R.J., Young, J.B. and Fantom, I.R., 1994, Modeling Alkali Salt Vapor Deposition in the British Coal Topping Cycle System. (The American Society of Mechanical Engineers, New York, NY, USA, GT-177).

Fluent. 2002, FLUENT User's Guide.).

Ganic, E.N. and Mastanaiah, K.M., 1981, Investigation of droplet deposition from a turbulent gas stream, Int J Multiphase Flow, 7: 401–422.

Greenfield, C. and Quarini, G., 1997, Particle deposition in a turbulent boundary layer, including the effect of thermophoresis, Proc. of the ASME Fluids Eng. Div. Summer Meeting, Gas Particle Flows.

Liu, D., Chen, P.L., Ji, L. and Rong, L.Z., 2003, Air duct cleaning-an effective way to improve indoor air quality, HV&AC, 33: 139–140 (in Chinese).

Liu, B.Y. and Agarwal, J.K., 1974, Experimental observation of aerosol deposition in turbulent flow, Aerosol Sci, 5: 145–155.

Lee, S.L. and Wiesler, M.A., 1987, Theory on transverse migration of particles in a turbulent two-phase suspension due to turbulent diffusion, Int J Multiphase Flow, 13: 99–111.

Launder, B.E., Reece, G.J. and Rodi, W., 1975, Progress in the development of a Reynolds-stress turbulent closure, J Fluid Mech, 68: 537–566.

Luo, Y.H., Yang, J. and Pan, W.M., 2003, Calculation of turbulent flow in 90° elbow pipe with square cross-section, Eng J Wuhan Univ, 36: 62–65 (in Chinese).

McLaughlin, J.B. 1989, Aerosol particle deposition in numerically simulated channel flow, Phys Fluids A, 1: 1211–1224.

Morsi, S.A. and Alexander, A.J., 1972, An investigation of particle trajectories in two-phase flow systems, J Fluid Mech, 55: 193–208.

Madabhushi, R.K. and Vanka, S.P., 1991, Large eddy simulation of turbulent-driven secondary flow in a square duct, Phys Fluids, 3: 2734–2745.

Papavergos, P.G. and Hedley, A.B., 1984, Particle deposition behaviour from turbulent flows, Chem Eng Res Des, 62: 275–295.

Pushkar, T.D. and Michael, A.A., 1998, Particle deposition from turbulent flow in a pipe, J Aerosol Sci, 29: 141–156.

Qian, C. and Goodarz, A.M., 1997, Deposition of particles in a turbulent pipe flow, J Aerosol Sci, 28: 789–796.

Rodi, W. 1984, Turbulent Models and their Application in Hydraulics. (IAHR, Delft, The Netherlands).

Sehmel, G.A. 1973, Particle eddy diffusivities and deposition velocities for isothermal flow and smooth surfaces, Aerosol Sci, 4: 125–138.

Shobokshy, M.S. 1983, Experimental measurements of aerosol deposition to smooth and rough surfaces, Atm Environ, 17: 639–644.

Saffman, P.G. 1965, The lift on a small sphere in a slow shear flow, J Fluid Mech, 22: 385–400.

Uijttewaal, W.S.J. and Oliemans, R.V.A., 1996, Particle dispersion and deposition in direct numerical and large eddy simulations of vertical pipe flows, Phys Fluids, 8: 2590–2604.

Wallin, O., 1994, Computer simulation of particle deposition in ventilating duct systems, Ph.D. Dissertation (Royal Institute of Technology, Stockholm, Sweden).

Wood, N.B. 1981, A simple method for the calculation of turbulent deposition to smooth and rough surfaces, J Aerosol Sci, 12: 275–290.

Wang, Q. and Squires, K.D., 1996a, Large eddy simulation of particle-laden turbulent channel flow, Phys Fluids, 8: 1207–1223.

Wang, Q. and Squires, K.D., 1996b, Large eddy simulation of particle deposition in a vertical turbulent channel flow, Int J Multiphase Flow, 22: 667–683.

White, F.M. 1986, Fluid Mechanics (2nd ed.), (McGraw-Hill, New York).

Yang, Z.W. and Lee, S.L., 1991, On the droplet deposition and mist supercooling in a turbulent channel flow, Part Syst Charact, 8: 72–78.

Zhang, H. and Ahmadi, G., 2000, Aerosol particle transport and deposition in vertical and horizontal turbulent duct flows, J Fluid Mech, 406: 55–80.